Astronomy & Astrophysics

XMM-Newton observation of the persistent Be/neutron star system X Persei at a high-luminosity level

N. La Palombara and S. Mereghetti

INAF – Istituto di Astrofisica Spaziale e Fisica Cosmica Milano, via Bassini 15, 20133 Milano, Italy
e-mail: nicola@iasf-milano.inaf.it

ABSTRACT

We report on the *XMM-Newton* observation of the HMXRB X Persei, the prototype of the persistent and low-luminosity Be/neutron star pulsars, which was performed in February 2003. The source was detected at a luminosity level of $\sim 1.4 \times 10^{35}$ erg s^{-1}, which is the highest level of the latest three decades. The pulsation period has increased to 839.3 s, thus confirming the overall spin-down of the neutron star detected in the previous observations. The folded light-curve has a complex structure, with features not observed at lower luminosities, and shows a significant energy dependence. The spectral analysis reveals the presence of a significant excess, at low energies, over the main power-law spectral component, which can be described by a black-body spectrum of high temperature ($kT_{\rm BB} \sim 1.5$ keV) and small emitting region ($R_{\rm BB} \sim 360$ m); its properties are consistent with a polar-cap origin. Phase-resolved spectroscopy shows that the emission spectrum varies along the pulse period, but it is not possible to prove whether the thermal component is pulsed or not.

1. Introduction

The X-ray source 4U 0352+309 is the brightest and perhaps most famous member of the Be/NS HMXRB class, whose optical counterpart was identified with the star X Persei (Braes & Miley 1972; van den Bergh 1972; Brucato & Kristian 1972; Weisskopf et al. 1984). In this system the companion pulsar accretes material from the massive, low-velocity equatorial wind of the Be primary star, and emits X-rays as the gravitational energy of the infalling material is converted to X-ray luminosity.

From the optical point of view, X Persei (HD 24534, HR 1209) is a bright star, highly variable (on time-scales from minutes to years) in optical and infrared (IR) brightness (V = 6.1–6.8, K = 5.2–6.7) and in emission-line strength (Mook et al. 1974; Roche et al. 1997). When the star is particularly bright, its spectrum displays strong emission in H$_\alpha$ and other Balmer lines, which marks this clearly as a Be-type system; when the star is faint, the emission lines disappear, and it appears to be a normal early-type star (see: Fabregat et al. 1992; Roche et al. 1997; and references therein). At times, it has also shown extreme, extended low states (Norton et al. 1991); during these periods the H$_\alpha$ line profile changed from emission to absorption, accompanied by a decrease in the IR flux by over a magnitude (Reynolds et al. 1992; Roche et al. 1993).

Such a variability is commonly thought to be caused by the formation and dissipation of a disk around the star, as observed for other Be stars. However, between 1994 and 1995, Liu & Hang (2001) observed that the H$_\alpha$ *EW* continued to increase even during the optical and near-infrared fading. They found that, although both components (line and continuum) arise from the same circumstellar envelope, their emissions peak at different evolution stages of the envelope itself, which correspond to different distances from the central star. In this scenario, the observed behavior of the two components is attributed to the

ejection of matter from the Be star as consecutive expanding rings.

The spectral class of the underlying OB star has been estimated to be O9.5 IIIe by Slettebak (1982). More recently Lyubimkov et al. (1997) have used both spectroscopic and photometric observations of the low-luminosity diskless phase of X Persei to infer the characteristics of the visible component; their results suggest a star of B0 Ve type, which is likely to have a mass of $\sim$13–20 $M_\odot$ and a radius of 5–10 $R_\odot$. With a projected equatorial velocity $v \sin i$ of $\sim$1200 km s^{-1} (Reynolds et al. 1992; Lyubimkov et al. 1997), the Be star is probably seen under a low or intermediate inclination angle.

Considering UV, optical and IR data taken in diskless and near-diskless states, Telting et al. (1998) modelled the stellar photosphere with $T_{\rm eff}$ = 31 000 K and $\log(g)$ = 4. They derived $E(B - V) = 0.39$ and, assuming $R_* = 9\ R_\odot$, estimated the distance to X Persei as 950 ± 200 pc. With a Galactic latitude of $-17°$, a distance estimate of $\sim$1 kpc implies that X Persei would be $\sim$300 pc from the Galactic plane. This is far from the plane compared to other early-type stars. However, it is within a few degrees of the plane of Gould's Belt, and the distance estimates for X Persei and the inferred extent of Gould's Belt ($\sim$600 pc; Torra et al. 2000) are marginally compatible.

The X-ray source has an unusually low luminosity; up to now it has varied on time-scales of years between $\sim$2.5 and $\sim$15 $\times 10^{34}$ erg s^{-1}. Moreover, while most Be/NS binary systems are transient in nature, 4U 0352+309 is a source of persistent X-ray emission. This is perhaps due to the relatively wide and nearly circular orbit of the system, whose complete ephemeris was determined by Delgado-Martí et al. (2001). They used measurements made with the *All Sky Monitor* (*ASM*) on *RossiXTE* to perform a pulse timing analysis of the 837 s pulsations, and found strong evidence for the presence of orbital Doppler delays. They inferred that the orbit is characterized by a period

P_{orb} = 250.3 days, a projected semimajor axis of the neutron star $a_x \sin i$ = 454 lt-s, a mass function $f(M)$ = 1.61 $M_\odot$ and an eccentricity e = 0.11. The measured orbital parameters, together with the known properties of the classical Be star X Persei, indicate a semimajor axis a = 1.8–2.2 AU and an orbital inclination $i \sim 26$–$33°$.

Pfahl et al. (2002) proposed this object as the prototype for a new class of HMXRBs characterized by long orbital periods (P_{orb} > 30 days) and low eccentricities. These systems are so wide that no tidal circularization can have occurred after the supernova explosion that created the neutron star, therefore all induced eccentricity must be primordial. While high velocity kicks are necessary to explain the eccentric orbits of most BeX transients (van den Heuvel & van Paradijs 1997), the low-e orbit of X Persei and of the other systems of its class must have formed in a supernova explosion without kick.

The 837 s pulsation period of 4U 0352+309 was discovered with the *Uhuru* satellite (White et al. 1976, 1977; Margon et al. 1977), and is still one of the longest periods of any known accreting pulsar (Bildsten et al. 1997; Haberl et al. 1998). The pulse profile of this source is almost sinusoidal. Some authors (Robba et al. 1996; Coburn et al. 2001) have reported the presence of structures in the hardness ratio (4–11 keV)/(1–4 keV), i.e., a sharp hardening episode corresponding to the pulse minimum and two softening episodes just before and after this hard spike.

Like many accreting pulsars, the history of the pulse period of 4U 0352+309 shows no evidence of a regular spin-up. For the first years after the discovery of pulsations, the pulsar exhibited apparently erratic pulse frequency variations on a time-scale of a few days, which were superposed on a long term trend in which it was spinning up at the rate of $\dot{P}/P = -1.5 \times 10^{-4}$ yr^{-1}. This was followed by a large apparent torque reversal around 1978. Since then, although the spin period measurements have been infrequent, the star has been spinning down at an average rate of $\dot{P}/P = 1.3 \times 10^{-4}$ yr^{-1} (White et al. 1976; Robba et al. 1996; di Salvo et al. 1998; Delgado-Martí et al. 2001, and references therein). In all, there have only been about two dozen determinations of the pulse period of 4U 0352+309, so its pulse period behavior on short time-scales (e.g., weeks, months, and even a year) is not well documented.

The transitions between the spin-up and spin-down stages occur without any significant variations of the system X-ray luminosity and, therefore, cannot be associated with the transitions of the neutron star between the accretor and propeller states. The long-term spin-down trend argues against the presence of a persistent accretion disk in this system; in contrast, the assumption of a spherical geometry in the accretion flow allows us to interpret the spin period of the neutron star in X Persei in terms of the equilibrium period, P_{eq}^{sph}, provided the average (on a time-scale of >20 yr) value of the wind velocity is 350–400 km s^{-1}. The spin-up/spin-down behavior of the source within this scenario can be associated with variations in the stellar wind velocity, which are due to the activity of the massive component and the orbital motion of the neutron star, whose trajectory is inclined to the plane of decretion disk of the Be companion (Ikhsanov 2007).

Another unusual aspect of 4U 0352+309 is its X-ray spectrum. Most accreting X-ray pulsar spectra are well described by a standard model, in which a simple power law with a photon index of ~1 is exponentially cut off above ~20 keV (White et al. 1983). The source 4U 0352+309, on the other hand, does not follow this standard spectral shape; it is possible that this is due to the low mass accretion rate. As a result, a variety of different models have been used to fit the spectrum. Using observations taken with *RossiXTE*, Coburn et al. (2001) found that all these models were improved by the addition of a cyclotron resonant scattering feature (*CRSF*) at ~29 keV. In particular, the model that best fitted the data is a combination of a blackbody plus a power law modified by a *CRSF* at 28.6 keV, which implies a magnetic field strength of $2.5(1 + z)10^{12}$ G in the scattering region (where z is the gravitational redshift). In the phase-averaged spectrum there is no evidence of a fluorescent Fe K-shell emission line in the range 6.4–6.7 keV, and the phase-resolved analysis shows that the blackbody and cyclotron line energies are consistent with being constant through the pulse.

Recently, Grundstrom et al. (2007) have observed that, between 2000 and 2006, the circumstellar disk grew to near record proportions, while at the same time, the system X-ray flux dramatically increased, presumably due to the enhanced mass accretion from the disk. The H$_\alpha$ emission equivalent widths were the largest measured over the last few decades (Roche et al. 1993; Piccioni et al. 2000; Clark et al. 2001), and they indicated that the disk had grown significantly. The apparent increase in X-ray flux that accompanied the disk expansion confirms that the X-ray source is powered by gas from the Be star disk. However, Grundstrom et al. (2007) found that the largest H$_\alpha$ half-maximum emission radius of the circumstellar disk was still much smaller than the separation between the Be star and neutron star. Therefore they suggested that tidal forces at periastron may excite a two-armed spiral in the disk, and that mass transfer will occur predominantly after periastron, as the gas in the arm extension is accreted by the neutron star. The observed phase of X-ray maximum, which occurs about one quarter of a period after periastron, is consistent with this picture.

2. Observations and data reduction

X Persei was observed by *XMM-Newton* for ~31 ks on February 2nd, 2003. The three *EPIC* cameras, i.e. one *pn* (Strüder et al. 2001) and two *MOS* (Turner et al. 2001), were active and operated in *Full Frame* mode. This gave time resolutions of 73 ms and 2.6 s. For all three cameras, the medium thickness filter was used. While in the case of the two *MOS* cameras the effective source exposure time is ~31 ks, it is much lower (~16 ks) for the *pn* camera, since it was affected by the "counting mode" effect during the observation.

We used version 7.0 of the *XMM-Newton Science Analysis System* (*SAS*) to process the event files. After the standard pipeline processing, we looked for possible periods of high instrumental background, caused by flares of soft protons with energies less than a few hundred keV. We found that the first ~20 ks of the observation were affected by a high soft-proton contamination. However, since X Persei was detected with a high count-rate (larger than 3 cts s^{-1} in each camera), much higher than that of the background, the soft-protons during the time intervals with high contamination have a negligible effect on the source spectral and timing analysis (their count rate in the source extraction area is less than 0.1 cts s^{-1}). Hence, for our analysis, we used the data of the whole observation.

3. Timing analysis

Due to the very high count rate, the data collected by the three *EPIC* cameras were highly affected by photon pile-up. For this reason, we had to exclude the central area of the source PSF and consider only data in an annulus area.
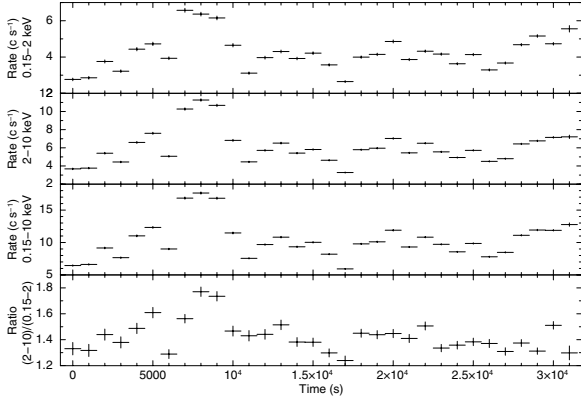
Fig. 1. Background subtracted light curves of X Persei in the energy ranges 0.15–2, 2–10, and 0.15–10 keV, with a time bin of 1 ks.
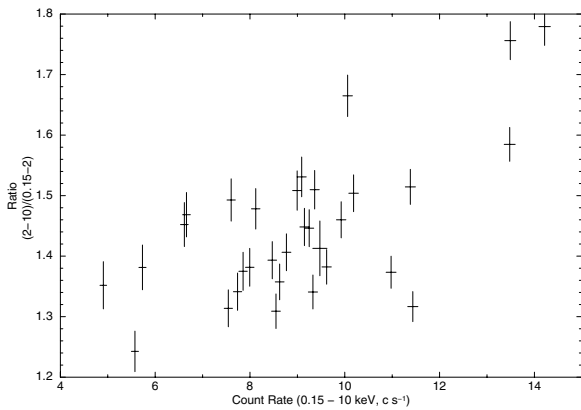

Fig. 2. Hardness-ratio variation of X Persei as a function of the 0.15–10 keV count rate, with a time bin of 1 ks.
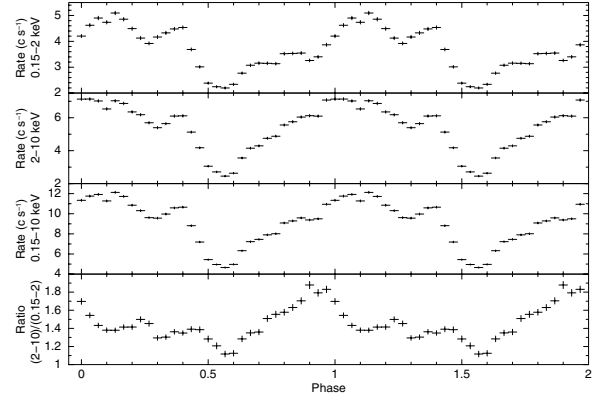

Fig. 3. Background subtracted light curves of X Persei in the energy ranges 0.15–2, 2–10, and 0.15–10 keV, folded at the best-fit period.
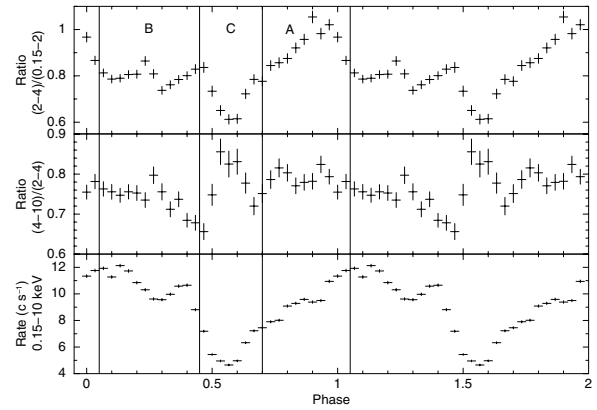

Fig. 4. Hardness ratios of the three light curves of X Persei in the energy ranges 0.15–2, 2–4, and 4–10 keV, as a function of the pulse phase. The vertical lines indicate the phase intervals used for the spectral analysis.

For the *MOS1* camera we selected an extraction corona with internal and external radii of 45 and 70″, respectively; for the *MOS2* camera the corresponding parameters are 40 and 70″. In the case of the *pn* camera the source was imaged close to a CCD gap, therefore we were forced to select a very narrow corona, with internal and external radii of 30 and 35″, respectively. We checked with the *SAS* task *epatplot* that, with these selections, no event pile-up affected our data, using them to accumulate the source light-curves. The background curves were accumulated on large circular areas with no sources and radii of 60″, 40″ and 45″ for the *MOS1*, *MOS2*, and *pn* cameras, respectively.

In Fig. 1 we report the total background-subtracted light curves in the 0.15–10 keV energy range. It shows that, during the *XMM-Newton* observation, there were significant flux changes in the source on a time-scale of several hours. Variations up to ∼50% around the average level of ∼10 cts s⁻¹ are evident. Moreover, the source *hardness-ratio* (HR) between the energy bands above and below 2 keV varies up to ∼30% around the average value of 1.45 and, over long time-scales, increases with the total count rate (Fig. 2).

To obtain a measure of the pulse period, we converted the arrival times to the solar system barycenter and performed a folding analysis using the source events of three cameras. In this way we derived a period of 839.3 ± 0.3 s. In Fig. 3 we show the folded light curves in the three energy intervals, 0.15–2, 2–10, and 0.15–10 keV, together with the folded HR between the hard and soft light curves. The pulse profile shows a main peak at phase ∼0–0.1, a secondary peak at phase ∼0.4, and a deep minimum at phase ∼0.5–0.6. The profile is energy-dependent,

because the main peaks are at phase ∼0 and ∼0.1 in the high and low energy ranges, respectively. Moreover, below 2 keV it shows a plateau in the phase range 0.7–0.9, which has no counterpart above 2 keV. This energy dependence is confirmed by the HR profile, the maximum of which is not aligned with that of the count-rate. The same plot also shows that there is not a simple correlation between the hardness and the total count rate; we observe the same HR value at completely different count rate levels, but also very different HR values for the same count rate. This indicates that the spectral hardness of X Persei does not depend in a simple way on its flux level.

We have also considered a finer energy division by dividing the hard energy range in the two sub-ranges 2–4 and 4–10 keV. In Fig. 4 we compare the folded *soft* and *hard* hardness ratios, i.e. the count-rate ratios in the energy bands (2–4)/(0.15–2) keV and (4–10)/(2–4) keV, respectively. In this way, we can show that the minimum of the first ratio (and of the total light-curve) coincides with the maximum of the second. This behavior was already observed by Robba et al. (1996) with the data collected in 1990 by the *GINGA* satellite.

4. Spectral analysis

For the source and background spectra, we considered the same extraction regions we used for the light curves. We accumulated all the events with pattern range 0–4 (i.e. mono– and bi-pixel events) and 0–12 (i.e. from 1 to 4 pixel events) for the *pn* and the two *MOS* cameras, respectively.
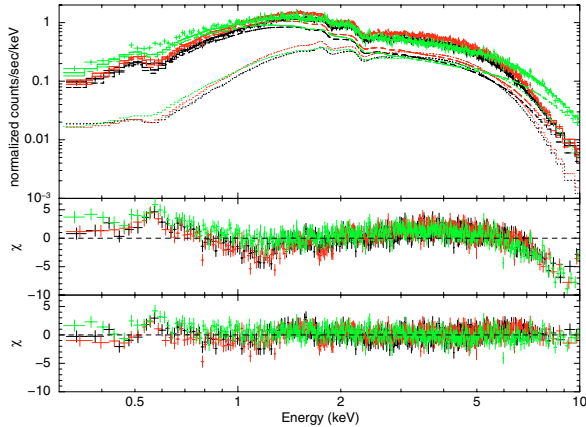
Fig. 5. *Top panel*: total spectrum of X Persei with the best-fit power-law (*dashed line*) plus black-body (*dotted line*) model. The spectra of the *MOS1*, *MOS2*, and *pn* cameras are shown in black, red and green, respectively. *Middle panel*: residuals (in units of σ) between data and model in the case of the single power-law. *Bottom panel*: residuals in the case of the power-law plus black-body.

Table 1. Best-fit parameters for the total spectrum of X Persei. The model parameters are the galactic interstellar absorption A_G, the main power-law component *PL*, the additional black-body component *BB* and the Gaussian line *GL*.

Component	Parameter	Value
A_G	N_H^a	$3.42^{+0.30}_{-0.08}$
PL	Γ	$1.48^{+0.02}_{-0.02}$
	Flux @ 1 keV^b	$9.48^{+0.64}_{-0.20}$
BB	kT(keV)	$1.42^{+0.04}_{-0.02}$
	R(m)^c	361^{+3}_{-3}
GL	E_{line}(keV)	$0.58^{+0.01}_{-0.04}$
	I_{line}^d	$2.13^{+0.22}_{-0.32}$
	EQW (eV)	97^{+10}_{-15}
d.o.f.		2126
χ_ν^2		1.021

^{a} 10^{21} cm^{-2}. ^{b} 10^{-2} ph cm^{-2} s^{-1} keV^{-1}. ^{c} For a source distance of 1 kpc. ^{d} 10^{-3} ph cm^{-2} s^{-1}.
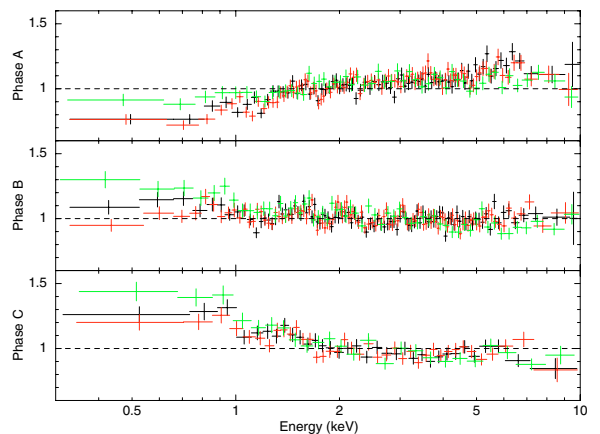

Fig. 6. Ratios of the spectra corresponding to the phase intervals shown in Fig. 4 to the average model spectrum. The parameters are fixed at the best-fit values for the total spectrum, except for the normalizations, which are at their best-fit values for each phase interval.

We generated ad hoc response matrices and ancillary files using the *SAS* tasks *rmfgen* and *arfgen*. In order to ensure the applicability of the χ^2 statistics, all spectra were rebinned with a minimum of 30 counts per bin; they were fitted in the energy range 0.3–10 keV using *XSPEC* 11.3.2. All spectral uncertainties and upper-limits are given at 90% confidence level for one interesting parameter.

After checking that separate fits of the three spectra gave consistent results, we fitted the spectra from the three cameras simultaneously, in order to increase the count statistics and to reduce the uncertainties. The fit with an absorbed power-law yielded $N_H = (3.56 \pm 0.05) \times 10^{21}$ cm^{-2} and photon index $\Gamma = 1.17 \pm 0.01$, but with large residuals and χ_ν^2/d.o.f. = 2.172/2131. The addition of a black-body component improved the fit quality significantly (Fig. 5): we obtained $N_H = (2.86 \pm 0.10) \times 10^{21}$ cm^{-2}, $\Gamma = 1.35 \pm 0.05$ and $kT_{BB} = 1.35 \pm 0.03$ keV, with χ_ν^2/d.o.f. = 1.052/2129. The emission surface of the thermal component has a radius $R_{BB} = 392^{+11}_{-10}$ m (for $d = 1$ kpc). The unabsorbed flux in the energy range 0.3–10 keV is $f_X \sim 1.2 \times 10^{-9}$ erg cm^{-2} s^{-1}, about 39% of which is due to the black-body component. Assuming a source distance of 1 kpc, this flux implies an unabsorbed source luminosity $L_X \sim 1.4 \times 10^{35}$ erg s^{-1}.

We also attempted to fit the spectra by replacing the black-body component with alternative emission models, such as *mekal*, thermal bremsstrahlung and broken power-law. In all these cases the results were worse than those obtained with the black-body model, since the reduced chi-squared was higher, the residuals were larger and/or the best-fit parameter values were unrealistic.

The spectra reported in Fig. 5 show that the best-fit model still leaves an emission feature at 0.5–0.6 keV. We could fit it with a Gaussian component at $E = 0.58$ keV, which has an equivalent width of 97 eV. On the other hand, we found no narrow iron K$_\alpha$ lines between 6 and 7 keV, and an upper limit on its equivalent width of 0.1 keV at most. The final best-fit parameters are reported in Table 1.

5. Phase-resolved spectroscopy

Due to the hardness-ratio variations observed along the pulse-period, we performed a phase-resolved spectroscopy in order

to study the source behavior in more detail. To this end, we analysed the background subtracted spectra in the three phase intervals defined in Fig. 4, i.e. 0.7–1.05 (phase A), 0.05–0.45 (phase B), and 0.45–0.7 (phase C).

The first step was to fit the three background subtracted spectra with the best-fit power law plus black-body model of the phase-averaged spectrum, leaving only the relative normalization factors free to vary. In Fig. 6 we report the ratios of the three spectra of each instrument to these renormalized average models. They show significant residuals for the spectra of phases A and C, which are harder and softer than the phase-averaged one, respectively. These ratios clearly demonstrate the spectral variability as a function of the pulse phase.

We then fitted the three spectra independently. In all cases, the absorbed power-law model was not satisfactory, while the addition of a black-body component significantly improved the fit. Therefore we used this model for all the spectra, leaving all the parameters free to vary; the results are reported in Table 2. They show that the absorbing column density is almost constant along the phase-pulse, as expected if it is due to the interstellar extinction. Moreover, neither the power-law nor the black-body components change significantly between phases A and B, either

Table 2. Best-fit spectral parameters for the phase-resolved spectroscopy of X Persei, in the case of the independent fit of the three spectra. Errors are at a 90% confidence level for a single interesting parameter. N_H, kT_{BB}, and R_{BB} are measured in units of 10^{21} cm^{-2}, keV, and meters (for a source distance of 1 kpc), respectively.

Spectral parameter	Phase interval		
	A	B	C
N_H	$3.23^{+0.19}_{-0.20}$	$2.67^{+0.14}_{-0.14}$	$2.94^{+0.28}_{-0.24}$
Γ	$1.30^{+0.09}_{-0.08}$	$1.32^{+0.06}_{-0.06}$	$1.61^{+0.17}_{-0.14}$
kT_{BB}	$1.36^{+0.05}_{-0.05}$	$1.28^{+0.05}_{-0.05}$	$1.48^{+0.06}_{-0.08}$
R_{BB}	425	433	264
f^a_{TOT}	1.46	1.49	0.82
f^a_{PL}	0.83	0.97	0.49
	(57 %)	(65 %)	(60 %)
f^a_{BB}	0.63	0.52	0.33
	(43 %)	(35 %)	(40 %)
χ^2_ν/d.o.f.	1.028/1465	1.032/1550	0.990/964

[a] Unabsorbed flux in the energy range 0.3–10 keV, in units of 10^{-9} erg cm^{-2} s^{-1}.

Table 3. Best-fit values for the black-body and power-law normalizations, when the three spectra are fitted simultaneously with common values of N_H ($2.94^{+0.09}_{-0.08} \times 10^{21}$ cm^{-2}), Γ ($1.40^{+0.04}_{-0.04}$) and kT_{BB} ($1.37^{+0.02}_{-0.02}$ keV). Errors are at a 90% confidence level for a single interesting parameter.

Spectral parameter	Phase interval		
	A	B	C
I^a_{PL}	70 ± 3	103 ± 3	67 ± 2
R^b_{BB}	465^{+11}_{-12}	388^{+10}_{-11}	247^{+10}_{-11}
f^c_{TOT}	1.43	1.50	0.84
f^c_{PL}	0.65	0.96	0.62
	(46%)	(64%)	(74%)
f^c_{BB}	0.78	0.54	0.22
	(54%)	(36%)	(26%)

[a] Intensity of the power-law component in units of 10^{-3} ph cm^{-2} s^{-1} keV^{-1} at 1 keV. [b] Radius of the black-body component (in metres) for a source distance of 1 kpc. [c] Unabsorbed flux in the energy range 0.3–10 keV, in units of 10^{-9} erg cm^{-2} s^{-1}.

Table 4. Best-fit values for the black-body and power-law normalizations, when the three spectra are fitted simultaneously with common values of N_H (($3.19^{+0.08}_{-0.08}$) $\times 10^{21}$ cm^{-2}), kT_{BB} ($1.38^{+0.02}_{-0.02}$ keV), and R_{BB} (376^{+9}_{-9} m for a source distance of 1 kpc). Errors are at a 90% confidence level for a single interesting parameter.

Spectral parameter	Phase interval		
	A	B	C
Γ	$1.21^{+0.02}_{-0.03}$	$1.44^{+0.03}_{-0.03}$	$2.16^{+0.07}_{-0.07}$
I^a_{PL}	85^{+2}_{-3}	112^{+3}_{-3}	64^{+3}_{-2}
f^b_{TOT}	1.51	1.51	0.85
f^b_{PL}	1.00	1.00	0.34
	(66%)	(66%)	(40%)
f^b_{BB}	0.51	0.51	0.51
	(34%)	(34%)	(60%)

[a] Intensity of the power-law component in units of 10^{-3} ph cm^{-2} s^{-1} keV^{-1} at 1 keV. [b] Unabsorbed flux in the energy range 0.3–10 keV, in units of 10^{-9} erg cm^{-2} s^{-1}.

in shape or in intensity. Instead there is a relevant variation in phase C; as the power-law component steepens, the black-body temperature increases and the total luminosity reduces.

For completeness, we also looked in the individual spectra for the presence of the emission Gaussian component at 0.58 keV, which was found in the phase-averaged spectrum. We found that this line is well defined in the spectra of phases B and C, with an equivalent width of ~105 and ~75 eV, respectively; on the other hand, it is not well constrained in phase A.

To investigate the relative variations of the two components with the period phase, we also simultaneously fitted the three spectra forcing common values for N_H, Γ and kT_{BB}. In this case we obtained $N_H = 2.94^{+0.09}_{-0.08} \times 10^{21}$ cm^{-2}, $\Gamma_{PL} = 1.40^{+0.04}_{-0.04}$ and $kT_{BB} = 1.37^{+0.02}_{-0.02}$ keV, with χ^2_ν/d.o.f. = 1.105/3989; the corresponding normalization values are reported in Table 3. In this interpretation, the spectral changes as a function of the phase are reproduced by the variations in the relative contribution of the two components. From this point of view, the power-law component provides the same flux during phases A and C, while it has a maximum during phase B. On the other hand, the contribution of the black-body component decreases progressively from phase A to phase C.

To confirm that the thermal component varies as a function of the rotational phase, we should prove that a constant black-body component is rejected by the data. To this end, we modified the test model by imposing a common value of both kT_{BB} and R_{BB} for the three spectra, while both Γ and I_{PL} could vary within them. The resulting best fit has $N_H = (3.19^{+0.08}_{-0.08}) \times 10^{21}$ cm^{-2}, $kT_{BB} = 1.38^{+0.02}_{-0.02}$ keV and $R_{BB} = 357^{+9}_{-9}$ m, while the power-law parameters are shown in Table 4. In this case the fit quality is very good (χ^2_ν/d.o.f. = 1.135/3989), comparable to that obtained in the previous case. Moreover, in this case we find that, during phase C, most (i.e. ~60%) of the total unabsorbed flux is due to the thermal component.

The above results are summarized in Fig. 7, where we show the pulse-phase dependence of the black-body temperature, the power-law photon index and the unabsorbed flux of the two components for both fits. Since they have a similar statistical quality, we can neither confirm nor deny that the thermal component is variable.

6. Discussion

In Fig. 8 we report the long-term evolution of X Persei luminosity and spin period since the first observations. The flux measured by *XMM-Newton* corresponds to ~10^{35} erg s^{-1}, which is the highest level of luminosity since the end of the outburst in 1975. This result is confirmed by the *RossiXTE/ASM* data, which are reported for comparison; they clearly indicate that the *XMM-Newton* observation was performed at a luminosity peak of the source, which was preceded by a steep increase and followed by a sharp decrease. This luminosity increase implies a corresponding increase in the accretion rate and, in the case of matter transfer to the NS via an accretion disk, a larger momentum transfer to the neutron star; therefore, we would expect to observe a pulsar spin-up. This is not confirmed by the measured pulse period, which is greater than in all the previous observations. The pulse period evolution shows that the pulsar spin-down has also proceeded during recent years, in spite of the luminosity increase. This is independent evidence that the matter is transferred from the Be companion to the NS without forming an accretion disk.

The analysis of the pulse profile between 0.15 and 10 keV shows that, contrary to previous findings (e.g. Robba et al. 1996; di Salvo et al. 1998; Coburn et al. 2001), at all energies, the pulse
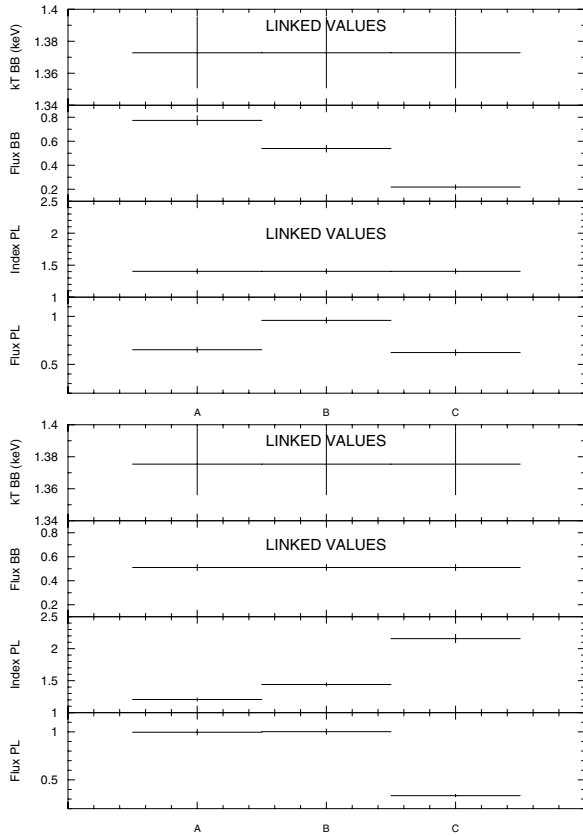
Fig. 7. Pulse-phase dependence of the black-body temperature, the power-law photon index and the unabsorbed flux of the two components (in units of 10^{-9} erg cm^{-2} s^{-1}), in the case of a common temperature and index (*top*) and of a common black-body (*bottom*).
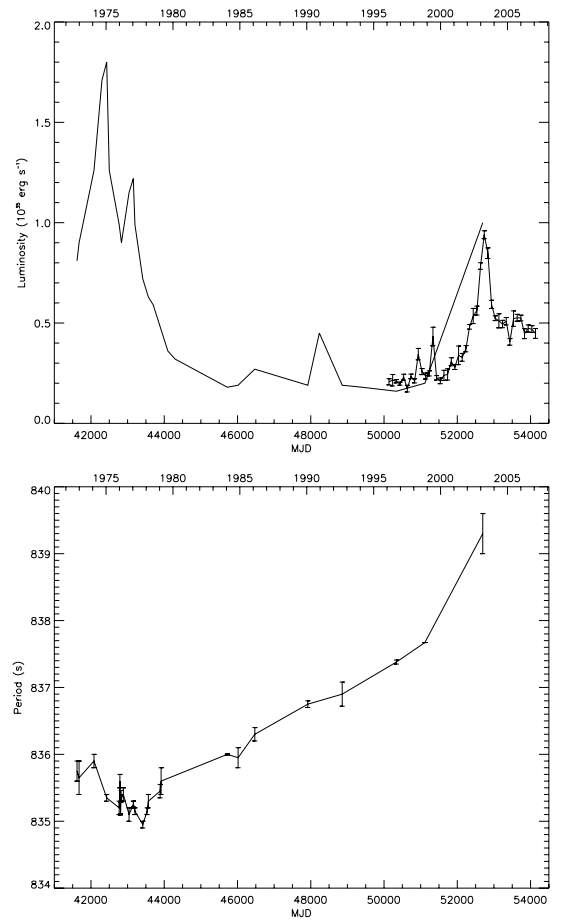

Fig. 8. Luminosity (*top*) and pulse-period (*bottom*) history of X Persei from 1972 October 29 to 2007 February 4. The luminosities of the top panel are based on the unabsorbed flux in the 2–10 keV and on a source distance of 1 kpc (Telting et al. 1998). The data with error-bars are based on *RossiXTE/ASM* measurements, which are reported for comparison.

shape is far from being sinusoidal. It has a rich structure, with a main and a secondary peak, and varies with the energy. As a consequence, the peak of the hardness ratio between the count rates above and below 2 keV is not aligned with the maximum of the total count rate. It is possible that this change in the pulse profile is due to the source luminosity level, which was higher than in all the previous detections. The analysis of the source status around the pulse minimum provided another interesting result; in this phase interval the hardness-ratio (2–4)/(0.15–2) reaches its minimum value, while the hardness-ratio (4–10)/(2–4) has a narrow peak. This behavior was previously observed by Robba et al. (1996) and Coburn et al. (2001) on *Ginga* and *RossiXTE* data, respectively, at lower luminosity levels (i.e. 2–5×10^{34} erg s^{-1}), and indicates a complex spectral evolution.

From the spectral point-of-view, we estimated a hydrogen column density $N_{\mathrm{H}} = (3.42^{+0.30}_{-0.08}) \times 10^{21}$ cm^{-2}, which is more than twice the value of $(1.51 \pm 0.22) \times 10^{21}$ cm^{-2} measured by Di Salvo et al. (1998) on *BeppoSAX* data. However, we showed that this difference is due to the different fit model they used (i.e. a high-energy cut-off power-law). For reference, we note that optical observations give $E(B - V) = 0.395$ (Telting et al. 1998); assuming $A_{\mathrm{V}} = 3.1 \, E(B - V)$ and the average relation $A_{\mathrm{V}} = N_{\mathrm{H}} \times 5.59 \times 10^{-22}$ cm^{-2} between optical extinction and X-ray absorption (Predehl & Schmitt 1995), this would predict $N_{\mathrm{H}} = 2.19 \times 10^{21}$ cm^{-2}.

It is interesting to compare our spectral results with those obtained by Coburn et al. (2001) on *RossiXTE* data, since these authors fit the source spectrum with a two component model equal to our model. They estimated a steeper power-law component ($\Gamma = 1.83 \pm 0.03$ instead of 1.48 ± 0.02), while the black-body

component had a comparable temperature ($kT = 1.45 \pm 0.02$ keV instead of $1.42^{+0.04}_{-0.02}$ keV). However, in our case the black-body radius is much larger (361 m instead of 130 m); this is not surprising, since during the *XMM-Newton* observation X Persei was about 5 times more luminous than during the *RossiXTE* observation. In spite of this luminosity difference, also in the case of the *RossiXTE* observation ∼60% of the total flux was due to the power-law component.

As in previous observations of X Persei, we found no evidence of an Fe-K line in the source spectrum. We estimated a 90% confidence upper limit on the equivalent width of almost 0.1 keV, i.e. an order of magnitude larger than in other studies. On the other hand, we found evidence of an emission line at 0.58 keV, which was never found before. It is rather weak (EQW = 97 eV) and was not detected in all the pulse-phases, therefore its analysis requires further investigation.

Coburn et al. (2001) performed a phase-resolved spectroscopy, with a different selection of the phase-intervals. Contrary to our findings, in their case both the power-law photon-index and the black-body temperature are almost constant along the pulse profile, and only the component normalizations change significantly. However, these results were obtained with much lower count statistics, and at a luminosity level about 5 times lower than in our case; furthermore, a fixed, common

value of the hydrogen column density was forced to the different spectral phases, and only data above 3 keV were considered.

The results we have obtained for X Persei are in agreement with what has been observed in two other Be/NS binaries with long pulse period, i.e. in the low luminosity system RX J0146.9+6121 (La Palombara & Mereghetti 2006) and during the low-luminous quiescent state of the transient source 3A 0535+262 (Orlandini et al. 2004; Mukherjee & Paul 2005). In these cases a thermal excess was detected above the main power-law; it has been modeled as a black-body with $kT_{BB} > 1$ keV and $R_{BB} < 1$ km, which contributes $\sim$30% of the total source luminosity. From this point of view, this class of low luminosity, long period Be/NS binaries is significantly different from the standard high-luminosity X-ray pulsars, whose thermal component is usually characterized by temperatures of $\sim$0.1 keV and radii of several hundred km (see La Palombara & Mereghetti 2006, for a review).

Hickox et al. (2004) showed that, in the low luminosity binary pulsars ($L_X \leq 10^{36}$ erg s^{-1}), the thermal component can be due to either emission by photo-ionized or collisionally heated diffuse gas, or to thermal emission from the surface of the neutron star. Based on our results, the first option can be rejected, since we cannot reconcile it with the observed black-body spectrum. We therefore favor the interpretation of the soft excess in X Persei as thermal emission from the neutron star polar cap. If we assume that the source is in the "accretor" status, with matter accretion on the NS surface, the black-body emitting radius of $\sim$360 m is consistent with the expected size of the polar cap. If $M_{NS} = 1.4\, M_{\odot}$ and $R_{NS} = 10^6$ cm, the source luminosity of 1.4×10^{35} erg s^{-1} implies an accretion rate $\dot{M} = 7.5 \times 10^{14}$ g s^{-1} and, adopting $B_{NS} = 10^{12}$ G, a magnetospheric radius $R_m = 8.4 \times 10^8$ cm (Campana et al. 1998). In this case, based on the relation $R_{col} \sim R_{NS}\,(R_{NS}/R_m)^{0.5}$ (Hickox et al. 2004), we would obtain $R_{col} \sim 345$ m, i.e. a value in agreement with the estimated black-body emitting radius.

Based on the above result, it makes sense to attribute the observed thermal component to the emission from the NS polar caps, as in the case of RX J0146.9+6121 and 3A 0535+262. If this description is correct, we would expect to observe some variability of the soft component along the pulse phase. From this point of view, the phase-resolved spectroscopy provides no conclusive results, since it proves that both a variable and a constant thermal component can account for the observed spectral variability.

7. Conclusions

Analyzing a $\sim$31 ks long *XMM-Newton* archival observation of the Be/NS binary system X Persei, we found that the source was detected at a luminosity level of $\sim$1.4 $\times 10^{35}$ erg s^{-1}, which is the highest value reported since the large outburst that occured in 1975. This result was independently confirmed by the *RossiXTE/ASM* data, which has been monitoring the source during the latest decade.

The timing analysis confirmed the pulsar spin-down already detected in the previous observations. Moreover, it shows that the pulse profile has a complex structure and is energy dependent.

From the spectral point-of-view, using the high effective area of *XMM-Newton* over a wide energy band, we could perform an accurate analysis at low energies. In this way, we detected a data excess above the main power-law component, which contributes $\sim$40% to the total source luminosity. Based on its black-body spectrum, with an emission radius of $\sim$360 m, this component

could be attributed to a polar-cap emission. It is interesting to note that the same hypothesis has also been advanced to describe the spectra of two other low-luminosity and long-period Be/NS pulsars, i.e. RX J0146.9+6121 and 3A 0535+262 (during its quiescent state).

We found no evidence of a narrow iron K$_\alpha$ line between 6 and 7 keV; on the other hand, our data suggest the presence of an emission feature at $\sim$0.58 keV, whose description and nature require further investigation.

The phase-resolved spectroscopy shows a large spectral variability along the pulse period, which can be modeled with both a variable and a constant thermal component. This result supports, but does not confirm, the polar-cap origin of this emission, therefore further studies will be necessary in the future to solve this issue.

References

Bildsten, L., Chakrabarty, D., Chiu, J., et al. 1997, ApJS, 113, 367
Braes, L. L. E., & Miley, G. K. 1972, Nature, 235, 273
Brucato, R. J., & Kristian, J. 1972, ApJ, 173, L105
Campana, S., Colpi, M., Mereghetti, S., Stella, L., & Tavani, M. 1998, A&ARv, 8, 279
Clark, J. S., Tarasov, A. E., Okazaki, A. T., Roche, P., & Lyuty, V. M. 2001, A&A, 380, 615
Coburn, W., Heindl, W. A., Gruber, D. E., et al. 2001, ApJ, 552, 738
Delgado-Martí, H., Levine, A. M., Pfahl, E., & Rappaport, S. A. 2001, ApJ, 546, 455
di Salvo, T., Burderi, L., Robba, N. R., & Guainazzi, M. 1998, ApJ, 509, 897
Fabregat, J., Reglero, V., Coe, M. J., et al. 1992, A&A, 259, 522
Grundstrom, E. D., Boyajian, T. S., Finch, C., et al. 2007, ApJ, 660, 1398
Haberl, F., Angelini, L., Motch, C., & White, N. E. 1998, A&A, 330, 189
Hickox, R. C., Narayan, R., & Kallman, T. R. 2004, ApJ, 614, 881
Ikhsanov, N. R. 2007, MNRAS, 375, 698
La Palombara, N., & Mereghetti, S. 2006, A&A, 455, 283
Liu, Q.-Z., & Hang, H.-R. 2001, Ap&SS, 275, 401
Lyubimkov, L. S., Rostopchin, S. I., Roche, P., & Tarasov, A. E. 1997, MNRAS, 286, 549
Margon, B., Thorstensen, J. R., Bowyer, S., et al. 1977, ApJ, 218, 504
Mook, D. E., Boley, F. I., Foltz, C. B., & Westpfahl, D. 1974, PASP, 86, 894
Mukherjee, U., & Paul, B. 2005, A&A, 431, 667
Norton, A. J., Coe, M. J., Estela, A., et al. 1991, MNRAS, 253, 579
Orlandini, M., Bartolini, C., Campana, S., et al. 2004, Nucl. Phys. B Proc. Suppl., 132, 476
Pfahl, E., Rappaport, S., Podsiadlowski, P., & Spruit, H. 2002, ApJ, 574, 364
Piccioni, A., Bartolini, C., Bernabei, S., et al. 2000, in The Be Phenomenon in Early-Type Stars, ASP Conf. Ser. 214, ed. M. A. Smith, H. F. Henrichs, & J. Fabregat, IAU Colloq., 175, 585
Predehl, P., & Schmitt, J. H. M. M. 1995, A&A, 293, 889
Reynolds, A. P., Hilditch, R. W., Bell, S. A., Pollacco, D. L., & Edwin, R. P. 1992, MNRAS, 258, 439
Robba, N. R., Burderi, L., Wynn, G. A., Warwick, R. S., & Murakami, T. 1996, ApJ, 472, 341
Roche, P., Coe, M. J., Fabregat, J., et al. 1993, A&A, 270, 122
Roche, P., Larionov, V., Tarasov, A. E., et al. 1997, A&A, 322, 139
Slettebak, A. 1982, ApJS, 50, 55
Strüder, L., Briel, U., Dennerl, K., et al. 2001, A&A, 365, L18
Telting, J. H., Waters, L. B. F. M., Roche, P., et al. 1998, MNRAS, 296, 785
Torra, J., Fernández, D., & Figueras, F. 2000, A&A, 359, 82
Turner, M. J. L., Abbey, A., Arnaud, M., et al. 2001, A&A, 365, L27
van den Bergh, S. 1972, Nature, 235, 273
van den Heuvel, E. P. J., & van Paradijs, J. 1997, ApJ, 483, 399
Weisskopf, M. C., Elsner, R. F., Darbro, W., et al. 1984, ApJ, 278, 711
White, N. E., Mason, K. O., Sanford, P. W., & Murdin, P. 1976, MNRAS, 176, 201
White, N. E., Mason, K. O., & Sanford, P. W. 1977, Nature, 267, 229
White, N. E., Swank, J. H., & Holt, S. S. 1983, ApJ, 270, 711